A Graph Neural Network Approach to Investigate Brain Critical States Over Neurodevelopment

Rodrigo M. Cabral-Carvalho [1,2], Walter H. L. Pinaya [2], João R. Sato [1]

[1] *Center of Mathematics, Computing and Cognition, Federal University of ABC, São Paulo, Brazil*

[2] *School of Biomedical Engineering & Imaging Sciences, King's College London, London, UK*

Abstract

Recent studies show that functional resting-state dynamics may be modelled by lattice models near criticality, such as the 2D Ising model. The Ising temperature, which is the control parameter dictating the phase transitions of the model, can provide insight into the large-scale dynamics and is being used to better understand different brain states and neurodevelopment. This period is categorized by intricated changes in the microcircuits to consolidate networks. These changes influence the macroscopic brain dynamics and also its functional relations, which can be observed in functional Magnetic Resonance Imaging (fMRI). Therefore, this work investigates neurodevelopment through a novel method to estimate the Ising temperature of the brain from fMRI data using functional connectivity and Graph Neural Networks (GNNs) trained on Ising model networks. The main finding indicates a statistically significant negative correlation between age and temperature for typically developing children ($r = -0.42$, $p < 0.001$) and also children with Attention-deficit/hyperactivity disorder (ADHD) ($r = -0.51$, $p < 0.001$). This study suggests that the brain gets distant from criticality as age increases, leading to a more ordered state.

Keywords: *functional connectivity, fMRI, neurodevelopment, graph neural networks, complex system.*

Author Summary

In this study, we employed Graph Neural Networks to investigate functional connectivity patterns of resting-state fMRI data using the 2D Ising model as a theoretical framework to access critical dynamics. Our key finding is the significant decrease in Ising temperature with age in both typically developing children and those with ADHD, indicating a developmental transition from a high-entropy, disordered state to a more ordered, decreasing the availability of dynamical states that the system can occupy and transit in different conditions. Moreover, this decrease in temperature is crucial as it implies that the brain is moving away from criticality leading the system to a more sub-critical regime. The correlation coefficients across the groups showed no significant differences, indicating the same developmental trajectory.

1 Introduction

The brain is organized in an astronomical scale network dominated by non-linear biochemical interaction which is also coupled with environmental information. This complex organization gives rise to various microscopic and macroscopic spatiotemporal patterns and cognitive, emotional, motor and sensorial behaviours (Kelso, S., 1995). The remarkable complexity of brain dynamics has been attracting the interest of eager physicists to model a set of equations that can give some perspective on self-organization and dynamical patterns. Thus, marvellous contributions propose brain dynamics as a collective process from microscopic components using tools from statistical physics and complex systems (Werner, 2007). One of the most

prominent results shows that resting state brain networks extracted from functional Magnetic Resonance Imaging (fMRI) BOLD-signal are statistically indistinguishable from ones extracted from the 2D Ising model, a mathematical and computational model from statistical physics to study phase transitions, showing that the macroscopic brain dynamics functionally operates near second-order phase transition elucidated by the 2D Ising model (Chialvo, 2010). This model explains magnetization as an emergent phenomena, known as spontaneous magnetization, using only collective microscopic interactions, which are controlled by a control parameter (Ising temperature). These emergent patterns appear at a very specific interval of values of the control parameter, which is the critical point, where the system is transitioning between two or multiple states (Beggs, 2008; Haimovici et al., 2013). Consequently, the concept that the brain operates near a critical point introduces the term "Critical Brain".

Despite the significant differences between the 2D Ising models, which consist of a simple two-dimensional lattice with local direct interactions ruled by a Hamiltonian, and the complex dynamics of the brain, it can provide some insights about whole-brain dynamics from the statistical physics perspective. It's important to remark that many studies invested in developing more improved Ising models for brain dynamics incorporating structural data (Nuzzi et al., 2020) and pairwise maximum entropy model (PMEM) and maximum likelihood estimation to infer parameters (e.g., interaction matrix J and external magnetic field h) given the data (Ezaki et al., 2017). However, using PMEM when the number of ROIs is large is still an issue (Ezaki et al., 2020). Therefore, this present work focuses on the simpler 2D Ising model, for the sake of creating an approach based on machine learning that operates at the connectivity level for inferring the temperature for 333 ROIs (i.e., a large number of ROIs) with a light computational cost for scalability over large datasets. Deep learning models can incorporate

various patterns and generalize over different dynamical systems (Legaard et al., 2023); thus, this work proposes an approach that can be extended to a deep learning model that learns from a variety of biologically informed and improved Ising models.

A geometric deep learning approach was employed to extract the complex features of connectivity information related to the Ising temperature in the network structure. This specialized Machine Learning algorithm approach operates on non-Euclidean spaces like networks. One of the most common approaches is the Graph Neural Network (GNN), which was trained using simulated 2D Ising model networks to predict the control parameter (Ising temperature) that originated the dynamics and consequentially, the connectivity graph. Therefore, once this geometric deep learning method was trained to correctly predict the Ising temperature, it was applied to estimate the temperature across neurodevelopment (ages 8 - 22 years) from rs-fcMRI graphs.

This period is heavily categorized by intricate changes in the microcircuits across the brain, especially in the cerebral cortex, to consolidate and create more cohesive networks (Paolicelli et al., 2011; Zuo et al., 2017). These significant changes influence the macroscopic brain dynamics and also its functional relations, which was observed in rs-fcMRI data, demonstrating mechanistic alterations on brain dynamics at the network level, representing a wide variety of neural patterns enabled by more flexible dynamics (Menon, 2013; Sydnor et al., 2021) and producing effects on the functional networks topological properties (Sato et al., 2016; Ernst et al., 2015; Betzel et al., 2014; Grayson & Fair, 2017; Soman et al., 2023). Thus, the absence of topological characterization of networks limits the analysis of studies where structural connectivity experiences significant changes. Therefore, due to the limitations of the 2D Ising

model with constant interactions and first neighbors coupling, the difference in critical state transitions using functional connectivity networks can only be assessed using Ising temperature.

In this context, this work examines neurodevelopment using Ising temperature to address how critical states relate to the formation and evolution of functional networks during neurodevelopment by the change in the control parameter. Indicating a departure from criticality over age, moving from a disordered phase to a more ordered one, where neural activity becomes less random and more predictable. Even though limited by a lack of topological characterization, the present framework inaugurates a computational light approach for large datasets, with many ROIs (i.e., 333), and extendable to diverse training sets extracted from various dynamical models to infer control parameters.

2 Results

2.1 Estimating Ising temperature during neurodevelopment

Once the GNN was trained on the Ising simulations, the Ising temperature of the rs-fMRI was estimated for Typically Developing Children and ADHD symptoms. Thus, the difference between the estimated Ising temperature T and the critical temperature Tc (T - Tc) was calculated. Hence, Pearson's and Spearman's Correlation were calculated, evidencing that both groups show a significant negative linear relationship between estimated temperature and age. For Typically Developing Children (Pearson = -0.42, $p < 0.001$; Spearman = -0.43, $p < 0.001$). For ADHD Symptom (Pearson = -0.51, $p < 0.001$; Spearman = -0.49, $p < 0.001$). Moreover, both groups are below the critical temperature Tc with a linear decrease in Ising temperature over

neurodevelopment (Fig. 1). Furthermore, to evaluate possible relations between Ising temperature with the main graph topology properties, a Pearson's correlation was used and can be found in the Supplementary Material (Table A).

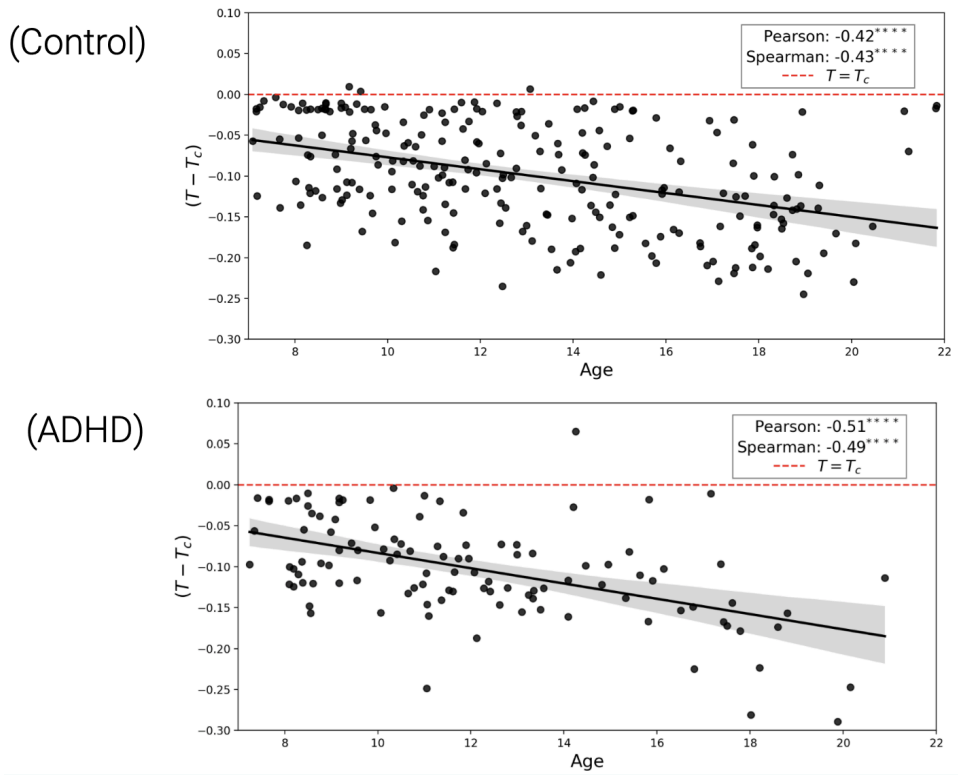

Figure 1. Estimated Ising temperature T minus critical temperature T_c plotted against age. The top plot (Control) shows typically developing children, and the bottom plot (ADHD) shows children diagnosed with Attention Deficit Hyperactivity Disorder (ADHD). The solid black line in each plot represents the linear trend between T - T_c and age, with a shaded region indicating the standard deviation. In both plots, a significant negative correlation between T - T_c and age is observed, as indicated by Pearson's correlation and Spearman's rank correlation values with corresponding asterisks denoting the level of statistical significance (**** $p \leq 0.0001$). The dashed red line represents the critical temperature T_c as a reference.

The age was divided into 7 groups of 2 years (7-9, 9-11, 11-13, 13-15, 15-17, 17-19, 19-21) and the distance of the estimated Ising temperature *T* to critical temperature *Tc* |T - Tc|

was calculated for each age group. As can be observed in Fig. 2, both typically developing children and subjects with ADHD symptoms are getting distant from criticality over neurodevelopment. Even though the median distance from the critical point always increases, not all groups are statistically different. Therefore, as expected, age groups distant in the age span show statistical significance. A two-sample t-test was used to assess differences in the distance to the critical temperature between age groups; the p-value for pairwise comparison between each group can be seen in Table 1.

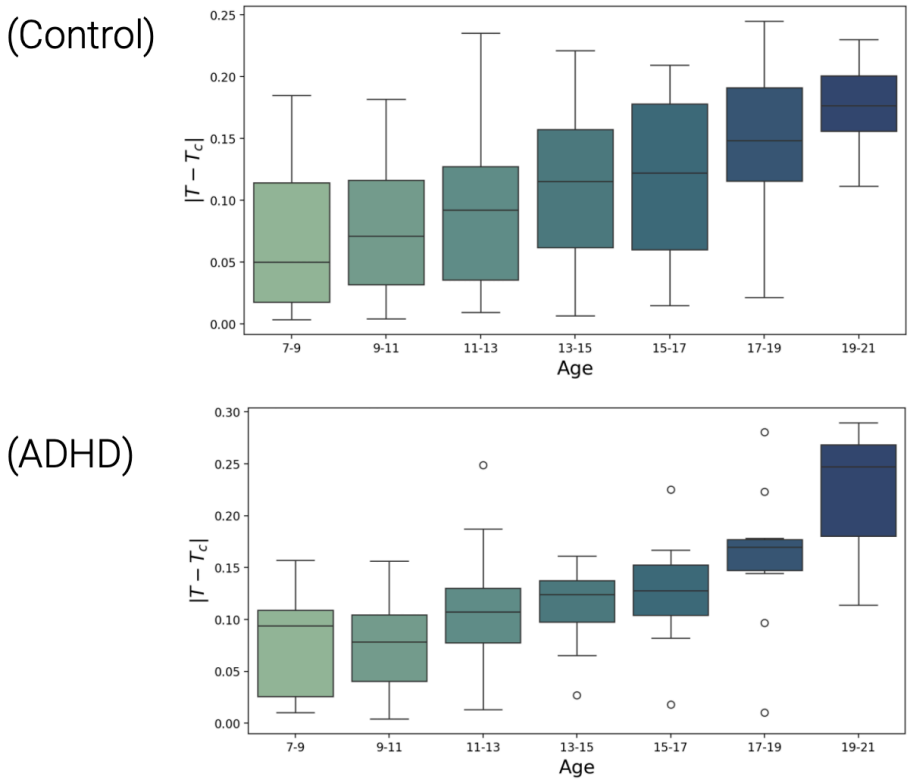

Figure 2. The box plots represent the distance from the estimated Ising temperature T to the critical temperature T_c (|T - Tc|) across age groups for both typically developing children (Control) and children with ADHD. The boxes show the interquartile range (IQR) with medians, and the error bars indicate data within 1.5 times the IQR. Circles represent outliers, which fall outside this range, particularly noticeable in the ADHD group for older age groups.

Age groups *p* values (Typically developing children)

	7-9	**9-11**	**11-13**	**13-15**	**15-17**	**17-19**	**19-21**
7-9	-	0.15	<0.001	<0.001	<0.001	<0.001	<0.001
9-11		-	0.16	<0.01	<0.01	<0.001	<0.001
11-13			-	0.14	0.07	<0.001	<0.001
13-15				-	0.6	0.02	<0.01
15-17					-	0.12	0.03
17-19						-	0.15
19-21							-

Age groups *p* values (ADHD Symptoms)

	7-9	**9-11**	**11-13**	**13-15**	**15-17**	**17-19**	**19-21**
7-9	-	0.89	0.12	0.01	0.001	<0.001	<0.001
9-11		-	0.01	<0.01	<0.001	<0.001	<0.001
11-13			-	0.69	0.41	0.02	<0.001
13-15				-	0.55	0.25	<0.001
15-17					-	0.24	0.05

17-19	-	0.28
19-21		-

Table 1. The paired t-test p-values results for the distribution of the distance from the estimated Ising temperature from the critical temperature for pairwise age groups. Top table - p-values for Typically developing children. Button table - p-values for ADHD symptoms.

2.2 Group differences

To evaluate the difference between the groups correlation coefficients, a bootstrap analysis was conducted to compare the distributions of the correlation coefficients for each group. This statistical technique involves repeatedly resampling the data with replacement to create a distribution of correlation coefficients, allowing for a more robust comparison between the groups. The analysis revealed that the presence of ADHD symptoms does not significantly affect the observed decrease in Ising temperature with age (Pearson's Correlation, $p = 0.5$; Spearman's Correlation, $p = 0.6$), indicating that the trend of the brain moving away from criticality as it matures is consistent regardless of ADHD status (Fig. 3).

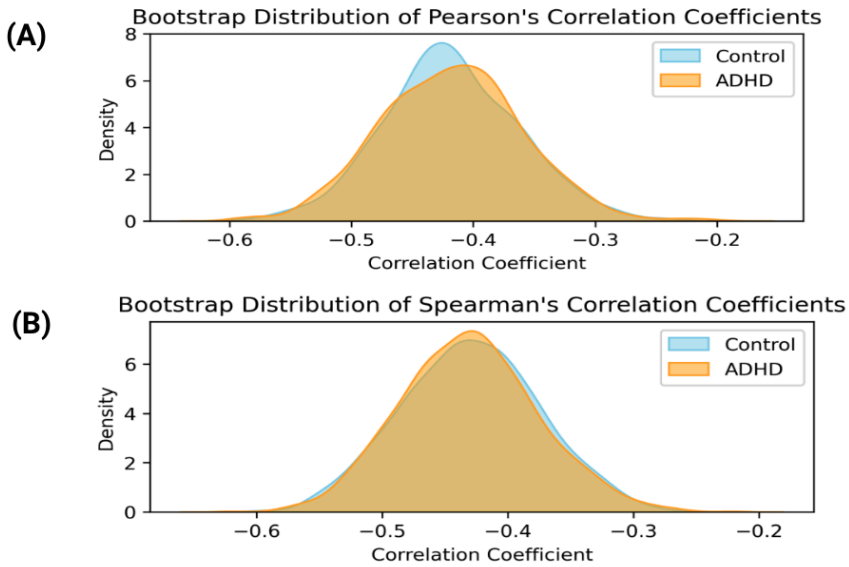

Figure 3. The bootstrap kernel density estimation (KDE) (*kernel = Gaussian; bandwidth = 1*), of correlation coefficients for control (blue) and ADHD (orange) groups. (A) Distribution of Pearson's Correlation Coefficients; (B)Distribution of Spearman's Correlation Coefficients. The overlap indicates that the presence of ADHD symptoms does not significantly affect the decrease in Ising temperature with age.

2.3 Confound analysis

To evaluate the influence of possible confounds, the effect of head motion was investigated on the Ising Temperate estimation since its significant impact on fMRI data (Friston et al., 1996). Thus, a linear regression was used to predict which variables could predict temperature (2 confounding variables: Max Motion (mm) and Max Rotation (degree), and Age (years) as the variable of interest), where Max Motion (mm), Max Rotation (degree) and Age (years) as independent variables and Estimated Ising temperature as the dependent variable, for each group. For the Typically Developing Children group model (R^2= 0.19) the only variable significant to explain the temperature was age and it's also negatively associated ($\beta = -0.43$, two-sided $p <$

0.001). For the ADHD symptom group model ($R^2 = 0.32$) the only variable significant to explain the temperature was age and it's also negatively associated ($\beta = -0.37$, two-sided $p < 0.001$). The results are shown in Table 2.

	Typically Developing Children		ADHD symptoms	
	β	p	β	p
Max Motion (mm)	-0.085	0.24	0.029	0.73
Max Rotation (degree)	-0.065	0.40	-0.033	0.65
Age	-0.434	< 0.001	-0.365	< 0.001
R^2	0.190		0.324	

Table 2. Linear regression summary (linear coefficient β, p-value and R^2) for the evaluation of head motion effects in Ising temperature estimation for Typically Developing Child and ADHD Symptoms Groups. A model was utilized for each group separately, using Max Motion (mm), Max Rotation (degree) and Estimated Ising temperature as features to explain the target variable Age (years).

3 Discussion

This paper is based on past research on complex systems, functional connectivity, and criticality, in particular, inspired by the evidence that the brain is poised near a second-order phase transition (Fraiman et al., 2009) and that brain criticality using Ising models can also be used to

investigate brain states (Ruffini et al., 2023, Kandeepan et al., 2020). The present framework assumes that the 2D Ising model can describe the empirical resting functional networks, as proposed by Fraiman et al. (2009), while expanding this concept over neurodevelopment. Thus, this work focuses on investigating brain criticality rather than characterizing changes in the topological organization of functional networks. Critical models have been a key to understanding the emergence of collective complex neural dynamics and can be clinically relevant to many domains – including anesthesia, sleep medicine, developmental-behavioural pediatrics, and psychiatry (Jiang et al., 2018; Zimmern, 2020; Rocha et al., 2022). During the critical phase, the model achieves an equilibrium between alignment interactions and thermal excitations (entropy gain). This equilibrium gives origin to the emergence of a diverse repertoire of complex patterns. Hence, estimating Ising temperature of rs-fMRI creates a bridge to investigate the availability of dynamical states that the system can occupy and transit in different conditions, such as neurodevelopment.

The main finding indicates a statistically significant negative correlation between age and Ising temperature for Typically Developing Children and ADHD symptoms, suggesting that the brain gets distant from criticality to an ordered state as age increases. Previous studies support that resting-state brain dynamics stay slightly below the critical point in a sub-critical regime (Skilling et al., 2019; Priesemann et al., 2014), however, this remains controversial, with other evidence showing a slight shift to a paramagnetic regime (Ezaki et al., 2020, Ruffini et al., 2023). However, different pre-processing pipelines and multiple co-factors could potentially influence the estimation and, therefore, the most valuable insights come from the overall trend. This present paper suggests a move from a disordered phase to a more ordered phase, where neural activity becomes less random and more predictable. The correlation coefficients for the groups

were statistically indistinguishable from each other, suggesting that the maturation process, as measured by the Ising temperature, follows a similar trajectory in both typically developing children and those with ADHD symptoms. This could be influenced by the use of medication in ADHD subjects. For both groups, possible motion confounds were excluded using linear regression analysis.

One of the most common frameworks to infer Ising temperature is based on the PMEM (Ruffini et al., 2023; Ezaki et al., 2017) that finds the appropriate probability distribution given data constraints. These techniques also allow the estimation of the coupling matrix **J,** which enables different strengths for interactions between spins, and the external magnetic field ***h***. Moreover, other studies also use the structural geometry of the brain as measured by diffusion tensor imaging to biologically inform the Ising model (Marinazzo et al., 2013; Kandeepan et al., 2020; Nuzzi et al., 2020). Even though most of these frameworks are more complex and robust, the model's fit is constrained by the ROI number and time point length, requiring much computational power to infer parameters for a large group of subjects with a wide number of ROIs (Ezaki et al., 2017). The present framework, based on machine learning, represents a simpler Ising model to compensate for these issues with the cost of several limitations: The coupling matrix **J** is constant for every spin, only direct neighbor interactions, the absence of the external magnetic field *h* and assume that the underlying model is capable of describing the empirical data. Despite the restrictions, the current approach can be improved and has significant differences and some advantages; it estimates the control parameter using directly from the connectivity information and has a very small computational cost after the training phase when inferring the Ising temperature from the connectivity matrix of a large group of subjects, respectively. Therefore, despite the present limitations and assumptions, the great advantage of

this framework is the scalability of estimating the Ising temperature for large datasets with a large number of ROIs.

Furthermore, it also contributes to a new methodology for functional connectivity, using graph-structured simulation data to train a neural network that is used in empirical data. This methodology proposes integrating theoretical models with empirical data once both brain networks and Ising networks share the graph structure. Thus, this framework benefits from the possibility of expansion for biology-inspired Ising models (Marinazzo et al., 2013; Kandeepan et al., 2020; Nuzzi et al., 2020) and other criticality models, such as the Kuramoto model, which addresses how individual components (oscillators or neurons) interact to produce collective states (Kitzbichler et al., 2009; Ponce-Alvarez et al., 2015). This gives the GNN the capability to learn complex data representations and extract information from the network topology to infer parameters. However, it is fundamental to address whether the simulation in which the machine learning method is trained can describe the empirical data to ensure a meaningful inference.

A significant limitation of this study that must be addressed is the absence of the topological characterization of the functional connectivity networks. While the 2D Ising model effectively captures functional resting state networks through the critical temperature without incorporating topological features (Fraiman et al., 2009), the current approach may overlook essential aspects of network reconfiguration that influence the brain's shift from disordered to more ordered states, weakening the results. Therefore, future models should aim to integrate topological metrics into the training set simulations and in post hoc analysis to ensure the completeness of the analysis.

4 Methods

4.1 Data description

For our study, we utilized the data provided by the Neuron Bureau for the Attention-deficit/hyperactivity disorder (ADHD) 200 competition. This dataset is public and was compiled from eight different centres. Resting-state fMRI data were acquired using 1.5 T scanners (detailed in Bellec et al., 2017). The dataset comprises 776 training subjects and 197 test subjects. The participants are categorized into four groups: healthy control, ADHD combined, ADHD hyperactive-impulsive, and ADHD inattentive. For the purpose of our analysis, we combined all ADHD types into a single category to focus on the binary classification between ADHD and healthy control participants. In addition to the basic fMRI data, various phenotypic information is provided for each subject, including age, gender, handedness, IQ, and ADHD type (Bellec et al., 2017). The head motion criteria, specifically head motion <3 mm translation or <3° rotation in any direction, were applied as per previous studies (Tamm et al., 2006; Ge et al., 2019). Therefore, to restrict the influence of head motion, this threshold was reduced to 1.5 mm and 1.5°, thus, the final number of subjects was 242 Typically developing children and 111 subjects with ADHD symptoms. The dataset was pre-processed using the Athena pipeline for resting-state fMRI and voxel-based morphometry preprocessing (grey matter) with AFNI and FSL (Bellec et al., 2017). The data, which include time course values of BOLD signals, were obtained from the Connectome website (www.preprocessed-connectomes-project.org/adhd200/). Preprocessing steps included removing the first four time points to allow for magnetization to reach equilibrium, slice time correction, motion correction, registration at 4x4x4 voxel resolution using Montreal Neurological Institute

(MNI) space, band-pass filtering (0.009 Hz < f < 0.08 Hz), and smoothing with a 6 mm FWHM Gaussian filter (for more details see Bellec et al., 2017). Each data collection site used its own scanner(s) and its own MR scanning parameters. Full details are available at ADHD-200-Webpage (2011). Only the first scan was considered for participants with multiple scans and selected 140 time points for every subject.

In order to minimize the risk of co-factors and co-foundings over age, the demographic information was evaluated. To remove the possibility of sex impact on age, the distribution was investigated (Male, 12.7 ± (3.8) years, Female, 12.4 ± (3.5) years) and also the ADHD impact on age (Typically Developing Children, 12.8 ± (3.7); ADHD-Combined, 11.6 ± (3.4); ADHD-Hyperactive/Impulsive, 14.4 ± (4.9); ADHD-Inattentive 11.9 ± (3.0)). Furthermore, motion was also evaluated, showing the max rotation (degree) has statistically significant Pearson's correlation value with age (Max rotation (degree), $r = -0.13$, *p-value* $= 0.01$ and Max motion (mm), $r = 0$, *p-value* > 0.05). Both distributions can be seen in Fig. 4.

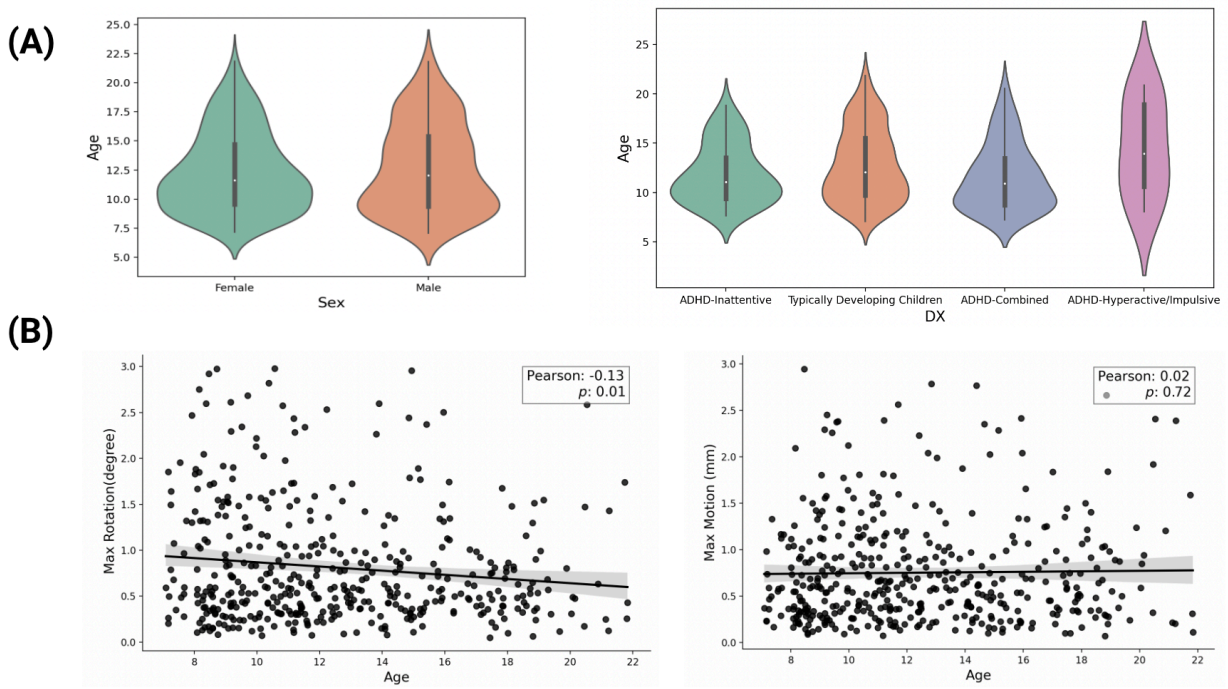

Figure 4. The main demographic aspects of the dataset. (A) The distribution of Sex of the four categories of participants, Typically Developing Children, ADHD-Combined, ADHD-Hyperactive/Impulsive, and ADHD-Inattentive, over age. (B) Scatter plot with Pearson's correlation and p-value for Max Rotation (degree) and Max Movement (mm), the solid black line in each panel represents the linear trend between head motion and age, with a shaded region indicating the standard deviation..

To better understand the influence of the presence of ADHD symptoms in motion, the dataset was separated into two groups; Typically Developing Children and ADHD Symptoms. Thus, the max motion (mm) and age for the ADHD group were the only statistically significant positive correlations (Max motion (mm) , Pearson's r = 0.27, p-value = 0.001; and Spearman's r = 0.25, p-value = 0.001). Both distributions can be seen in Fig. 5.

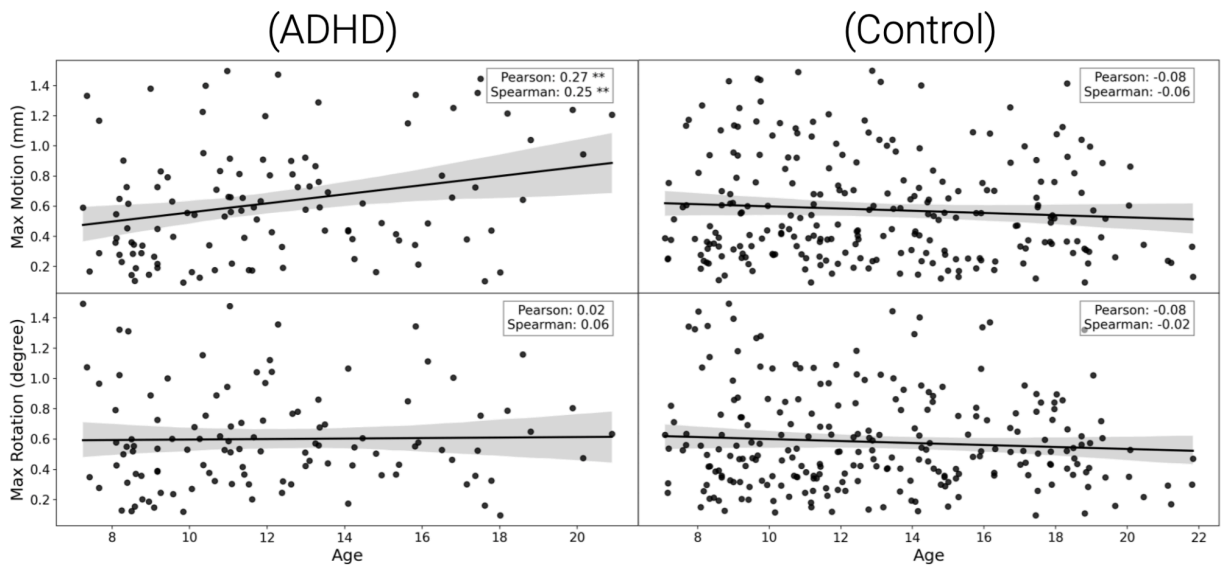

Figure 5. Scatter plots showing Pearson's correlation and p-values for Max Movement (mm) and Max Rotation (degrees) as a function of age in children diagnosed with ADHD (left) and Typically Developing children (right). The top row represents Max Movement (mm), while the bottom row represents Max Rotation (degrees). Each scatter plot includes a linear trend line (solid black) with the shaded region indicating the standard deviation. Pearson's correlation coefficient and Spearman's rank correlation are displayed in each panel, with asterisks denoting the significance levels (* $p < 0.05$, ** $p < 0.01$, *** $p < 0.001$).

4.2 Image Processing

The functional data was parcellated into 333 cortical regions of interest (ROIs), as defined by (Gordon et al., 2016). This parcellation was motivated by the intense changes the cortex undergoes during neurodevelopment (Baum et al., 2020) and by the intrinsic critical nature of cortical networks (Páscoa dos Santos et al., 2023). Then, we obtained the average BOLD signal of the voxels in each ROI. Pearson's pairwise correlation of different ROIs was calculated to create the adjacency matrix A (connectivity matrix). Therefore, a brain graph is defined as $\boldsymbol{G = (V, E, A)}$, with $\boldsymbol{V = \{1, ..., N\}}$ a set of nodes (or vertices), E representing a set of corresponding

edges, and $\mathbf{A} \in \mathbf{R}^{NxN}$ denoting the weighted adjacency matrix. One entry $\boldsymbol{w_{ij}}$ of the adjacency matrix **A** would indicate the connection strength (Pearson's Correlation) between node $\boldsymbol{i}$ and node $\boldsymbol{j}$ of graph $\boldsymbol{G}$.

4.3 2D Ising model Simulation

The 2D Ising model describes ferromagnetic materials and demonstrates magnetization resulting from a second-order phase transition. The model consists of a grid of spins, which are described by a discrete variable that takes two values $\sigma_i = -1, 1$, that is, spin "up" and spin "down", and the interaction of these spins without an external magnetic field is given by Hamiltonian (McCoy et al., 1973),

$$H = -\sum_{i,j} J\, \sigma_i \sigma_j$$

where $\sum_{i,j}$ represents the sum of neighbouring spins and J is the coupling constant that describes how strong is the interaction between the spins. Using $H = E$, it is possible to obtain energy information for any state of the grid.

Given the discrete and stochastic nature of the Ising model, Monte Carlo algorithms are convenient for calculating some model estimates. More specifically, the algorithm Metropolis-Hastings (Gould and Tobochnik, 1996; Metropolis et al., 1953). The algorithm is built based on the concept of Markov chains (see Supplementary Material for more details). All simulations were performed on a lattice $L = 250$, starting with all spins aligned or else randomly distributed, with Monte Carlo time steps $\Delta t = L \times L$ to cover all sites in the network giving the chance for every spin to change its state at least once (Fraiman et al., 2009). The 2D

Ising model undergoes a second-order phase transition when passing through the critical temperature $T_c \approx 2.269J$ (McCoy et al., 1973). The Boltzmann constant and the coupling constant are set to $k_\beta = J = 1$.

The 2D Ising model was simulated using a lattice of 250×250 spins fluctuating over 200 time steps after thermal equilibrium, where each time step allows all the spins of the lattice to change their state. Once the model is indeed in thermal equilibrium, the lattice is averaged over blocks of 13×13 spins, in order to get a continuous time series representative of the fMRI signal (Fig. 6). Since 250 is not divisible by 13, a floor division is applied, which means extracting just the integer part of a division. This reduces the system to a smaller grid where each block is averaged, resulting in a lattice of 250//13 x 250//13 = 19 x 19, which contains 361 ROIs. Now we calculate the correlation matrix and then remove the excess rows and columns to get 333 sizes. The full correlation matrix is initially larger (361 x 361), but the target is a smaller matrix (333 x 333). By calculating how many rows and columns to remove from each side, the code extracts the central portion of the matrix, removing 14 rows and columns from both the top and bottom, as well as the left and right, ensuring the final matrix has the desired dimensions. This helps to eliminate boundary effects. The 2D Ising model graphs were calculated by the resulting in 333 nodes (the simulation and processing are open-source, available on https://github.com/Rodrigo-Motta/BRAIN_ISING_GNN).

It is important to remark that each time step in the averaged lattice represents the collective behaviour of populations of (13x13) spins changing their states. This impacts not only the spatial resolution of the system but also the temporal relationships. In the initial Ising model, a time step is defined as $\Delta T = L \times L$. After the spatial average the new size of the model is $L' = L//13$ and the time interval of the averaged model is $\Delta T = L \times L \approx 169(L' \times L')$. In

short, every step in the averaged lattice results from many interactions of the original model since we now have populations of spins.

To check that the 2D Ising model simulation routine was correctly employed and thermalized, in the absence of an external magnetic field, the order parameter (mean magnetization per site) was evaluated in a wide range of $[1.6,\ 3.3]\ k_{\beta}T/J$. For model robustness, the evaluation was conducted for three different lattice sizes compared with the analytical solution. The chosen lattice size was selected based on less variability during the critical regime and dimensionality proximity with Gordon's parcellation of 333 ROIs.

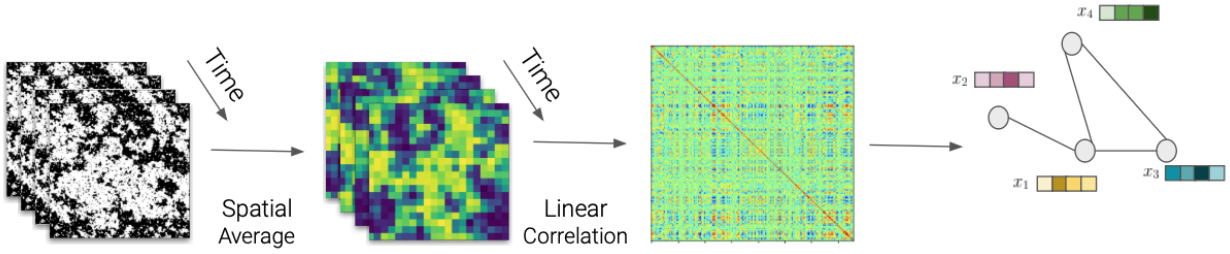

Figure 6. The creation of 2D Ising model networks process. Firstly, the spatial average of near spins results in a continuous version of the simulated dynamical 2D Ising Model. Then, a pairwise Pearson's correlation is calculated over all lattices to create the graph adjacency matrix with the same dimensionality as the rs-fMRI connectivity matrix.

4.4 Graph Convolutional Neural Networks (GCNs)

The GCN mechanism can be described by convolution operations, non-linear activation functions, pooling, and backpropagation. Firstly, the graph convolution operation is the primary operation of a GCN, extracting topological structures from the graph. This operation is based on a message-passing operation (for more details, see Supplementary Material). These intrinsic

geometric operations from GCNs allow the complex representation learning and prediction of global parameters from networks. In this work, this model learns to estimate a global property of the graph by extracting and transforming connectivity features from nodes by graph convolutional layers (Kipf & Welling, 2016).

Even though GNN operates in graph structures, it's necessary to process the graphs for the GNN. Thus, the k-nearest neighbors (KNN) algorithm was used to determine the graph edges to connect each node and its neighbors. This approach effectively avoided problems with fitting noise and vanishing gradients , where each node represented an ROI and the node features were the connectivity with the other ROIs (Qin et al., 2022; Lei et al., 2022). A GCN was trained to calculate the Ising temperature for the brain networks, with three graph convolutional layers, a global average pooling process, and two linear layers. The activation function was the Leaky-Retified Linear Unit (Leaky-ReLu) in order to allow negative correlation values, the dropout technique was also used, and the loss function used was the Mean Absolute Error (MAE) with L2 Regularization to avoid overfitting. The architecture can be seen in Fig. 7.

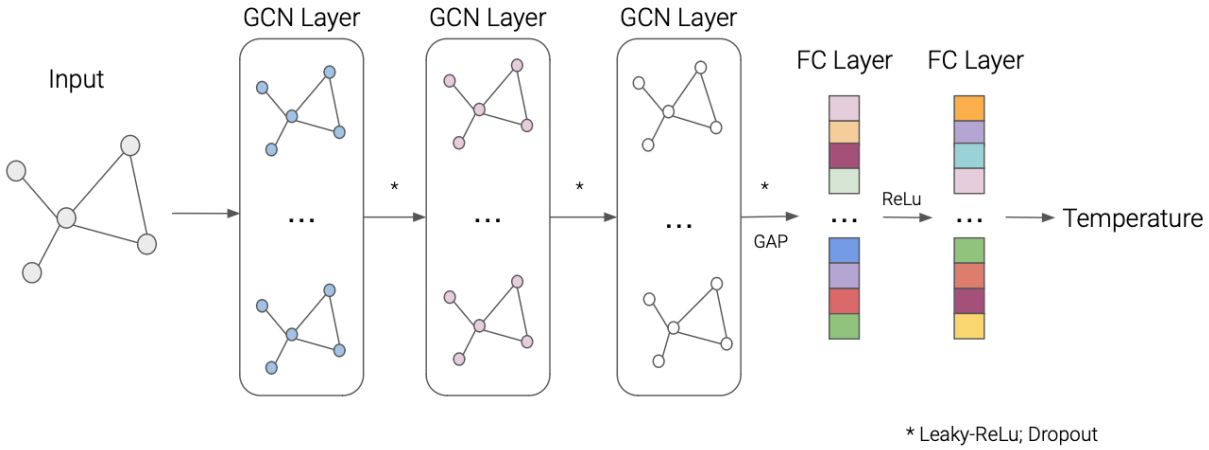

Figure 7. Overview of the GCN regressor architecture. Firstly, the input, a graph extracted from the ising model or empirical data, passes through 3 successive GCN layers, followed by a GAP and two successive FC layers to map

the Ising temperature. Abbreviations: GAP, global average pooling; Leaky-ReLu, Leaky-Retified Linear Unit; FC, Fully Connected.

The dataset used for modeling was composed of 1500 simulations of the 2D Ising model uniformly distributed around the critical point (Temperature interval = $[1.8,\ 2.5]$), where 1000 simulations were used to train the network, 250 to evaluate and 250 to test. The GNN was trained over 100 epochs, using a Cycle Optimization technique; this method varies the learning rate according to triangle waves with selected maximum and minimum. In this specific work, a threshold of loss was used in the validation set to select a good candidate of minima to fine-tune the model in order to increase accuracy.

4.5 Using GNN to estimate Ising temperature

The input to a GNN is inherently a graph structure, which allows for the effective analysis of data with complex relationships. Given that both the brain and Ising model graphs share the same dimensionality, the trained GNN can seamlessly process both types of data. This dimensional consistency ensures that the model, once trained on the Ising model graphs, can be effectively used to estimate the temperature of brain graphs. This capability allows the GNN to generalize its learned representations from simulated data to real-world fMRI data. Thus, this methodology enables estimation between theoretical model parameters and empirical data. The overview of the methodology can be seen in Fig. 8.

Once the GNN was trained on the 2D Ising model simulations around criticality ([1.8, 2.4] k_BT/J) and the hyperparameter-tuning was done on the validation set to optimize

performance. The GNN efficiency predicting the temperature on the test set was $MAE = 0.04$ and $R^2 = 0.92$.

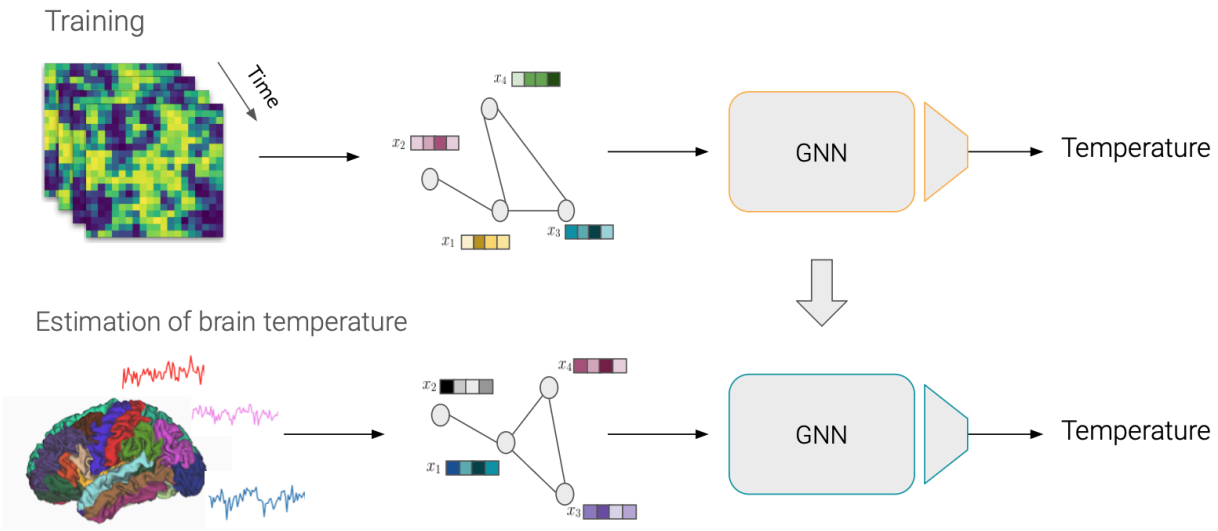

Figure 8. Overview of the methodology. On the top, the training phase of the Graph Neural Network (GNN) used multiple simulated Ising model networks in different temperatures to create a regressor. On the bottom, the trained GNN is used to estimate the Ising temperature using whole brain networks.

4.6 Statistical Analysis

Firstly, to evaluate the overall trend of the temperature over age, a Pearson's correlation and Spearm's rank correlation were used. A bootstrap was done to check the statistical differences between correlation coefficients between groups (ADHD and Control). The bootstrap analysis was implemented using 1000 resamples, following the bias-corrected and accelerated bootstrap (see Details in Efron et al., 1996). In each repetition, the correlation coefficient was computed, and the resampling was performed with replacement, where the average percentage of subjects excluded in each resample is 36.8%, following the probability of not being chosen. The

confidence level was set at 95%, meaning the resulting bootstrap confidence interval covers the true correlation coefficient approximately 95% of the time.

To check possible differences in temperature between different age groups, the data was separated in 7 groups of 2 years (7-9, 9-11, 11-13, 13-15, 15-17, 17-19, 19-21). The percentage distribution of data across the age groups is as follows: The age group 9-11 has the highest percentage at 20.17%, followed closely by the 11-13 group at 19.75%. The 13-15 group accounts for 16.39%, while the 7-9 group represents 15.55%. The age group 17-19 makes up 15.13%, and the 15-17 group comprises 9.66%. Lastly, the 19-21 age group has the smallest percentage, accounting for 3.36% of the total data.

Data and Code Availability

All software and procedures concerning the analysis were detailed in the methods and supplementary materials and are available at GitHub https://github.com/Rodrigo-Motta/BRAIN_ISING_GNN. The dataset, which includes time course values of BOLD signals, was obtained freely on (http://fcon_1000.projects.nitrc.org/indi/adhd200/).

Author Contributions

Conceptualization: R.C., J.R. Data curation: R.C., J.R. Methodology: R.C., W.P., J.R. Investigation: R.C., W.P., J.R. Resources: R.C., J.R Formal analysis: R.C., J.R Visualization: R.C. Writing—original draft: R.C., J.R. Writing—review & editing: R.C., J.R. Project

administration: J.R. Software: R.C. Visualization: R.C. Supervision: W.P., J.R. Funding acquisition: R.C., J.R.

Acknowledgments

This study is supported by the São Paulo Research Foundation (FAPESP) Grants 2021/05332- 8, 2023/02616-0, 2023/02538-0 and 2024/00861-0.

Declaration of Competing Interest

The authors declare no conflicts of interest or competing interests.

References

Baum, G. L., Cui, Z., Roalf, D. R., Ciric, R., Betzel, R. F., Larsen, B., Cieslak, M., Cook, P. A., Xia, C. H., Moore, T. M., Ruparel, K., Oathes, D. J., Alexander-Bloch, A. F., Shinohara, R. T., Raznahan, A., Gur, R. E., Gur, R. C., Bassett, D. S., & Satterthwaite, T. D. (2020). Development of structure-function coupling in human brain networks during youth. *Proceedings of the National Academy of Sciences of the United States of America, 117*(1), 771–778. https://doi.org/10.1073/pnas.1912034117

Beggs, J. M. (2008). The criticality hypothesis: How local cortical networks might optimize information processing. *Philosophical Transactions. Series A, Mathematical, Physical, and Engineering Sciences, 366*(1864), 329–343. https://doi.org/10.1098/rsta.2007.2092

Bellec, P., Chu, C., Chouinard-Decorte, F., Benhajali, Y., Margulies, D. S., & Craddock, R. C. (2017). The Neuro Bureau ADHD-200 preprocessed repository. *NeuroImage, 144*, Part B, 275–286. https://doi.org/10.1016/j.neuroimage.2016.06.034

Betzel, R. F., Byrge, L., He, Y., Goñi, J., Zuo, X. N., & Sporns, O. (2014). Changes in structural and functional connectivity among resting-state networks across the human lifespan. *NeuroImage, 102* Pt 2, 345–357. https://doi.org/10.1016/j.neuroimage.2014.07.067

Chialvo, D. (2010). Emergent complex neural dynamics. *Nature Physics, 6*, 744–750. https://doi.org/10.1038/nphys1803

Defferrard, M., Bresson, X., & Vandergheynst, P. (2016). Convolutional neural networks on graphs with fast localized spectral filtering. *NIPS 2016 final revision*. arXiv:1606.09375. https://doi.org/10.48550/arXiv.1606.09375

Efron, B., & Tibshirani, R. J. (1993). *An introduction to the bootstrap.* Chapman & Hall/CRC. (Monographs on Statistics and Applied Probability, No. 57).

Ernst, M., Torrisi, S., Balderston, N., Grillon, C., & Hale, E. A. (2015). fMRI functional connectivity applied to adolescent neurodevelopment. *Annual Review of Clinical Psychology, 11*, 361–377. https://doi.org/10.1146/annurev-clinpsy-032814-112753

Ezaki, T., Fonseca dos Reis, E., Watanabe, T., & others. (2020). Closer to critical resting-state neural dynamics in individuals with higher fluid intelligence. *Communications Biology, 3*(52). https://doi.org/10.1038/s42003-020-0774-y

Ezaki, T., Watanabe, T., Ohzeki, M., & Masuda, N. (2017). Energy landscape analysis of neuroimaging data. *Philosophical Transactions. Series A, Mathematical, Physical, and Engineering Sciences, 375*(2096), 20160287. https://doi.org/10.1098/rsta.2016.0287

Fraiman, D., Balenzuela, P., Foss, J., & Chialvo, D. R. (2009). Ising-like dynamics in large-scale functional brain networks. *Physical Review E, 79*(6), 061922. https://doi.org/10.1103/PhysRevE.79.061922

Friston, K. J., Williams, S., Howard, R., Frackowiak, R. S., & Turner, R. (1996). Movement-related effects in fMRI time-series. *Magnetic Resonance in Medicine, 35*(3), 346–355. https://doi.org/10.1002/mrm.1910350312

Ge, R., Torres, I., Brown, J. J., Gregory, E., McLellan, E., Downar, J. H., et al. (2019). Functional disconnectivity of the hippocampal network and neural correlates of memory impairment in treatment-resistant depression. *Journal of Affective Disorders, 253*, 248–256. https://doi.org/10.1016/j.jad.2019.04.096

Grayson, D. S., & Fair, D. A. (2017). Development of large-scale functional networks from birth to adulthood: A guide to the neuroimaging literature. *NeuroImage*, 160, 15-31. https://doi.org/10.1016/j.neuroimage.2017.01.079

Gordon, E. M., Laumann, T. O., Adeyemo, B., Huckins, J. F., Kelley, W. M., & Petersen, S. E. (2016). Generation and Evaluation of a Cortical Area Parcellation from Resting-State Correlations. *Cerebral cortex (New York, N.Y. : 1991)*, *26*(1), 288–303. https://doi.org/10.1093/cercor/bhu239

Gould, H., & Tobochnik, J. (1996). *An introduction to computer simulation methods.* Addison-Wesley.

Haimovici, A., Tagliazucchi, E., Balenzuela, P., & Chialvo, D. R. (2013). Brain organization into resting state networks emerges at criticality on a model of the human connectome. *Physical Review Letters, 110*(17), 178101. https://doi.org/10.1103/PhysRevLett.110.178101

Jiang, L., Sui, D., Qiao, K. *et al.* (2018). Impaired Functional Criticality of Human Brain during Alzheimer's Disease Progression. *Sci Rep* 8, 1324. https://doi.org/10.1038/s41598-018-19674-7

Kandeepan, S., Rudas, J., Gomez, F., Stojanoski, B., Valluri, S., Owen, A. M., Naci, L., Nichols, E. S., & Soddu, A. (2020). Modeling an auditory stimulated brain under altered states of consciousness using the generalized Ising model. *NeuroImage, 223*, 117367. https://doi.org/10.1016/j.neuroimage.2020.117367

Kelso, S. (1995). *Dynamic patterns: The self-organization of brain and behavior.* The MIT Press.

Kipf, T. N., & Welling, M. (2017). Semi-supervised classification with graph convolutional networks. *Published as a conference paper at ICLR 2017*. arXiv:1609.02907. https://doi.org/10.48550/arXiv.1609.02907

Kitzbichler, M. G., Smith, M. L., Christensen, S. R., & Bullmore, E. (2009). Broadband criticality of human brain network synchronization. *PLOS Computational Biology, 5*(3), e1000314. https://doi.org/10.1371/journal.pcbi.1000314

Legaard, C., Schranz, T., Schweiger, G., Drgoňa, J., Falay, B., Gomes, C., Iosifidis, A., Abkar, M., & Larsen, P. (2023). Constructing neural network based models for simulating dynamical systems. *ACM Computing Surveys, 55*(11), Article 236. https://doi.org/10.1145/3567591

Lei, D., Qin, K., Pinaya, W. H. L., Young, J., Van Amelsvoort, T., Marcelis, M., Donohoe, G., Mothersill, D. O., Corvin, A., Vieira, S., Lui, S., Scarpazza, C., Arango, C., Bullmore, E., Gong, Q., McGuire, P., & Mechelli, A. (2022). Graph convolutional networks reveal network-level functional dysconnectivity in schizophrenia. *Schizophrenia Bulletin*, 48(4), 881-892. https://doi.org/10.1093/schbul/sbac047

López-Vicente, M., Agcaoglu, O., Pérez-Crespo, L., Estévez-López, F., Heredia-Genestar, J. M., Mulder, R. H., Flournoy, J. C., van Duijvenvoorde, A. C. K., Güroğlu, B., White, T., Calhoun, V.,

Marinazzo, D., Pellicoro, M., Wu, G. R., Angelini, L., Cortes, J. M., & Stramaglia, S. (2013). Information transfer of an Ising model on a brain network. *BMC Neuroscience*, 14(Suppl 1), P376. https://doi.org/10.1186/1471-2202-14-S1-P376

McCoy, B. M., & Wu, T. T. (1973). *The two-dimensional Ising model.* Harvard University Press. https://doi.org/10.4159/harvard.9780674180758

Menon, V. (2013). Developmental pathways to functional brain networks: Emerging principles. *Trends in Cognitive Sciences*, 17(12), 627-640. https://doi.org/10.1016/j.tics.2013.09.015

Metropolis, N., Rosenbluth, A. W., Rosenbluth, M. N., Teller, A. H., & Teller, E. (1953). Equation of state calculations by fast computing machines. *Journal of Chemical Physics, 21*(6), 1087. https://doi.org/10.1063/1.1699114

Nuzzi D, Pellicoro M, Angelini L, Marinazzo D, Stramaglia S. (2020). Synergistic information in a dynamical model implemented on the human structural connectome reveals spatially distinct associations with age. *Network Neurosci*ence ;4(3):910-924. https://doi.org/10.1162/netn_a_00146

Paolicelli, R. C., Bolasco, G., Pagani, F., Maggi, L., Scianni, M., Panzanelli, P., Giustetto, M., Ferreira, T. A., Guiducci, E., Dumas, L., Ragozzino, D., & Gross, C. T. (2011). Synaptic pruning

by microglia is necessary for normal brain development. *Science, 333*(6048), 1456–1458. https://doi.org/10.1126/science.1202529

Páscoa dos Santos, F., Vohryzek, J., & Verschure, P. F. M. J. (2023). Multiscale effects of excitatory-inhibitory homeostasis in lesioned cortical networks: A computational study. *PLOS Computational Biology,* 19(7), e1011279. https://doi.org/10.1371/journal.pcbi.1011279

Ponce-Alvarez, A., Deco, G., Hagmann, P., Romani, G. L., Mantini, D., & Corbetta, M. (2015). Resting-state temporal synchronization networks emerge from connectivity topology and heterogeneity. *PLoS computational biology*, *11*(2), e1004100. https://doi.org/10.1371/journal.pcbi.1004100

Priesemann, V., Wibral, M., Valderrama, M., Pröpper, R., Le Van Quyen, M., Geisel, T., Triesch, J., Nikolić, D., & Munk, M. H. (2014). Spike avalanches in vivo suggest a driven, slightly subcritical brain state. *Frontiers in Systems Neuroscience, 8*, 108. https://doi.org/10.3389/fnsys.2014.00108

Qin, K., Lei, D., Pinaya, W. H. L., Pan, N., Li, W., Zhu, Z., Sweeney, J. A., Mechelli, A., & Gong, Q. (2022). Using graph convolutional network to characterize individuals with major depressive disorder across multiple imaging sites. *EBioMedicine, 78*, Article 103977. https://doi.org/10.1016/j.ebiom.2022.103977

Rocha, R. P., Koçillari, L., Suweis, S., & others. (2022). Recovery of neural dynamics criticality in personalized whole-brain models of stroke. *Nature Communications, 13*, 368. https://doi.org/10.1038/s41467-022-30892-6

Ruffini, G., Damiani, G., Lozano-Soldevilla, D., Deco, N., Rosas, F. E., Kiani, N. A., Ponce-Alvarez, A., Kringelbach, M. L., Carhart-Harris, R., & Deco, G. (2023). LSD-induced increase of Ising temperature and algorithmic complexity of brain dynamics. *PLOS Computational Biology, 19*(2), e1010811. https://doi.org/10.1371/journal.pcbi.1010811

Sato, J. R., Biazoli, C. E., Salum, G. A., Gadelha, A., Crossley, N., Vieira, G., Zugman, A., Picon, F. A., Pan, P. M., Hoexter, M. Q., Anés, M., Moura, L. M., Del'Aquilla, M. A. G., Junior, E. A., McGuire, P., Rohde, L. A., Miguel, E. C., Bressan, R. A., & Jackowski, A. P. (2016). Connectome hubs at resting state in children and adolescents: Reproducibility and psychopathological correlation. *Developmental Cognitive Neuroscience, 20*, 2–11. https://doi.org/10.1016/j.dcn.2016.05.002

Skilling, Q. M., Ognjanovski, N., Aton, S. J., & Zochowski, M. (2019). Critical dynamics mediate learning of new distributed memory representations in neuronal networks. *Entropy, 21*(11), 1043. https://doi.org/10.3390/e21111043

Soman, S. M., Vijayakumar, N., Thomson, P., Ball, G., Hyde, C., & Silk, T. J. (2023). Functional and structural brain network development in children with attention deficit hyperactivity disorder. *Human Brain Mapping, 44*(8), 3394–3409. https://doi.org/10.1002/hbm.26288

Sydnor, V. J., Larsen, B., Bassett, D. S., Alexander-Bloch, A., Fair, D. A., Liston, C., Mackey, A. P., Milham, M. P., Pines, A., Roalf, D. R., Seidlitz, J., Xu, T., Raznahan, A., & Satterthwaite, T. D. (2021). Neurodevelopment of the association cortices: Patterns, mechanisms, and implications for psychopathology. *Neuron, 109*(18), 2820–2846. https://doi.org/10.1016/j.neuron.2021.06.016

Tamm, L., Menon, V., & Reiss, A. L. (2006). Parietal attentional system aberrations during target detection in adolescents with attention deficit hyperactivity disorder: Event-related fMRI evidence. *American Journal of Psychiatry, 163*(6), 1033–1041. https://doi.org/10.1176/ajp.2006.163.6.1033

Tiemeier, H., & Muetzel, R. L. (2021). Developmental changes in dynamic functional connectivity from childhood into adolescence. *Frontiers in Systems Neuroscience, 15*, 724805. https://doi.org/10.3389/fnsys.2021.724805

The ADHD-200 Consortium. (2012). The ADHD-200 Consortium: A model to advance the translational potential of neuroimaging in clinical neuroscience. *Frontiers in Systems Neuroscience, 6*, 62. https://doi.org/10.3389/fnsys.2012.00062

Werner, G. (2007). Brain dynamics across levels of organization. *Journal of Physiology - Paris, 101*(4–6), 273–279. https://doi.org/10.1016/j.jphysparis.2007.12.001

Zimmern, V. (2020). Why brain criticality is clinically relevant: A scoping review. *Frontiers in Neural Circuits, 14*, 54. https://doi.org/10.3389/fncir.2020.00054

Zuo, X. N., He, Y., Betzel, R. F., Colcombe, S., Sporns, O., & Milham, M. P. (2017). Human connectomics across the life span. *Trends in Cognitive Sciences, 21*(1), 32–45. https://doi.org/10.1016/j.tics.2016.10.005

Supplementary Material

Temperature and global graph properties

Despite the difficulty of describing changes in network topology in Ising Temperature, relationships can be explored by verifying Pearson's correlation with other global graph metrics within the groups. Thus, some main graph topological properties were used: Average clustering, average betweenness centrality, average path length, average degree, and average degree standard deviation. Therefore, the temperature change is strongly correlated to all measures except for average betweenness centrality in both groups.

	Control		*ADHD*	
Metric	*r*	*p*	*r*	*p*
Average Clustering	*0.73*	*<0.0001*	*0.78*	*<0.0001*
Average Betweenness Centrality	*0.07*	*0.2*	*-0.07*	*0.4*
Average Path Length	*0.63*	*<0.0001*	*0.7*	*<0.0001*

Average Degree	*0.82*	*<0.0001*	*0.85*	*<0.0001*
Average Degree Standard Deviation	*0.75*	*<0.0001*	*0.72*	*<0.0001*

Table A. Pearson's correlation between Ising Temperature changes and global graph metrics. The table presents the metrics, Pearson correlation coefficients (r) and the corresponding p-values (p) for the relationship between changes in the estimated Ising Temperature and various graph topological properties, including Average Clustering, Average Betweenness Centrality, Average Path Length, Average Degree, and Average Degree Standard Deviation.

2D Ising model simulation

The 2D Ising model describes ferromagnetic materials in a simplified way using just one free parameter (Temperature). This model shows magnetization resulting from a phase transition, and it consists of a grid of spins, which are described by a discrete variable that takes two values $\sigma_i = -1, 1$, and the interaction of these spins given by Hamiltonian in the absence of external magnetic field (McCoy et al., 1973),

$$H = -\sum_{i,j} J\, \sigma_i\, \sigma_j$$

J is the coupling constant and $\sum_{i,j}$ is the sum of the nearest neighboring spins. When set $H = E$, it is possible to obtain energy information for any lattice configuration or state of the grid. To solve the 2D Ising model the algorithm Metropolis-Hastings is used considering as an isolated system (Gould and Tobochnik, 1996; Metropolis et al., 1953). The algorithm is built based on the concept of Markov chains, which is a stochastic model that describes a sequence of possible events in which the probability of each event depends only on the state reached in the previous

event. A Markov process is solely by the transition probabilities $P(X_{n+1} = \mu \mid X_n = \nu)$, that is the probability of going to μ from ν. In this way, the entire process can be reduced to a matrix ***P*** that contains the information to go from one state to another in one step. From these properties, it follows that for a matrix ***P***, the Markov process will have a distribution stationary station that follows the balance equation,

$$\frac{P(\mu|\nu)}{P(\nu|\mu)} = \frac{\pi(\mu)}{\pi(\nu)}.$$

That is, the probability of transition from μ ν being in ν is equal to the probability of transition from ν μ being in μ. Rewriting this relation as

$$P(\mu|\nu)\pi(\nu) = P(\nu|\mu)\pi(\mu).$$

To simulate the Ising model, it is enough to know $\pi(x)$. Using the canonical and immediate ensemble,

$$\pi(x) = p(x) = \frac{1}{Z}e^{-\beta E_x}$$

where $Z = \Sigma\, i\, exp(-\beta Ei)$ is the partition function and $\beta = 1/(k_\beta T)$ (McCoy et al., 1973). This way, the balance equation is achieved,

$$\frac{P(\mu|\nu)}{P(\nu|\mu)} = \frac{\pi(\mu)}{\pi(\nu)} = e^{-\beta\Delta E}$$

where $\Delta E = (E_{\mu} - E_{\nu})$. Changing the value of a single variable changes its state, or the ΔE flip of a spin in position (i, j) will be just the energy difference in its neighbors since it will not change the energy at any other point on the grid. Therefore, considering the power before the flip

$$E_{n} =- J\sigma_{(i,j)}[\sigma_{(i+1,j)} + \sigma_{(i-1,j)} + \sigma_{(i,j+1)} + \sigma_{(i,j-1)}].$$

After rotating the spin $\bar{\sigma}_{(i,j)}$ the energy will be given by

$$E_{n+1} =- J\bar{\sigma}_{(i,j)}[\sigma_{(i+1,j)} + \sigma_{(i-1,j)} + \sigma_{(i,j+1)} + \sigma_{(i,j-1)}].$$

Therefore, the variation in energy of rotating the spin

$$E_{flip} =- 2J\sigma_{(i,j)}[\sigma_{(i+1,j)} + \sigma_{(i-1,j)} + \sigma_{(i,j+1)} + \sigma_{(i,j-1)}].$$

With the balance equation E_{flip} calculated, it is possible to create an iterative routine to simulate the model.

(1) First, we call a state, then we rotate a spin randomly on the grid and calculate the energy E_{flip};

(2) If the energy increases, we define $P(\mu \rightarrow \nu) = 1$, by the equilibrium equation, the spin inverts again mind if $P(\mu \rightarrow \nu) = exp(-\beta\Delta E)$;

(3) If the energy decreases, then $P(\nu \rightarrow \mu) = 1$ the state remains with the spin turned;

(4) Repeat this process for all spins.

The simulations were performed on a lattice $L = 250$, starting with all spins aligned or else randomly distributed, with Monte Carlo time steps $\Delta t = L \times L$ to cover all sites in the network, giving, on average, the chance of each spin of the lattice changing its state (Fraiman et al., 2009). Furthermore, as the grid is finite, the spins that are located on the edges are linked by the periodic boundary condition, in which the spins on the right edge interact with the left edge spins. With Onsager's analytical solution for the case $h = 0$ with no external magnetic field, it was discovered that the 2D Ising model undergoes a second-order phase transition when passing through the critical temperature $T_c = 2J/(ln(1) + \sqrt{2}) \approx 2.269J$ (McCoy et al., 1973). The Boltzmann constant and the coupling constant are set to $k_\beta = J = 1$.

In the simulation, a (250 x 250) lattice is divided into blocks of size 13. Since 250 is not divisible by 13, a floor division is applied, which means extracting just the integer part of a division. This reduces the system to a smaller grid where each block is averaged, resulting in a lattice of 250//13 x 250//13 = 19 x 19, which contains 361 ROIs. Now, we calculate the correlation matrix and then remove the excess rows and columns to get 333 size. The full correlation matrix is initially larger (361 x 361), but the target is a smaller matrix (333 x 333). By calculating how many rows and columns to remove from each side, the code extracts the central portion of the matrix, removing 14 rows and columns from both the top and bottom, as well as the left and right, ensuring the final matrix has the desired dimensions. This helps to eliminate boundary effects.

Graph Neural Networks (GNNs)

In order to define a graph convolution operation, it's important to define a graph as $G = (V, E, A)$, where V denotes a set of $|V| = N$ nodes (or vertices), E represents a set of corresponding edges, and $A \in R^{NxN}$ denotes the *weighted adjacency matrix*. One entry ω_{nm} of the adjacency matrix A would indicate the Pearson's Correlation between the time series of the node n *a*nd node m of a graph G. The graph must also have a feature matrix X in order to be processed by a GCN, which, in this specific case X **,** is also the connectivity matrix; therefore, this graph can be fully explained by the adjacency matrix.

The GCN mechanism can be described by convolution operations, non-linear activation functions, pooling, and backpropagation. Firstly, the graph convolution operation is the primary operation of a GCN, extracting topological structures from the graph. This operation is based on a message passing operation, which can be simply defined as

$$f(X) = \sigma(\overline{A}XW)$$

Where $\overline{A}$ is the normalized adjacency matrix**,** X the feature matrix, W **is** the learnable parameter matrix, and σ is a non-linear function (Defferard et al., 2016; Kipf & Welling, 2016). The normalized adjacency matrix solves the problem of feature values for nodes with many neighbors; this summation embedded in the matrix multiplication can overestimate nodes with a high degree. Therefore, it's common to solve this problem using the degree matrix using a symmetric normalization as follows:

$$\overline{A} = D^{(-1/2)}AD^{(-1/2)}$$

Where D is the diagonal degree matrix of A. This normalized adjacency matrix $\overline{A}$ is then multiplied by the node feature matrix X and the learnable matrix W, propagating node features across the graph and updating X for $f(X)$. Each layer updates the node features with dimensionality reduction in the bottleneck design. The convolutional operation in graphs is similar to the convolution operation in CNNs but is applied to the graph's adjacency matrix instead of a regular grid. Unlike filters in Convolutional Neural Networks (CNNs), our weight matrix W is unique and shared among every node.